Novel Circulating Fluidized-Bed Membrane Reformer for the Efficient Production of Ultraclean Fuels from Hydrocarbons

Pradeep Prasad* and Said S. E. H. Elnashaie

Chemical Engineering Department, 230 Ross Hall, Auburn University, Auburn, Alabama 36849

An integrated novel fluidized-bed membrane steam reformer for the efficient production of hydrogen is proposed and investigated. It consists of two connected subsystems, viz., a circulating fluidized-bed membrane reformer and a reactor−regenerator for dry reforming. The steam-reforming part is an extension of the previous successful work regarding a bubbling fluidized-bed membrane reformer. The fast fluidization regime is more efficient and productive than the bubbling regime. Hydrogen-permeable membranes to remove hydrogen are used together with a CO_2 acceptor to remove carbon dioxide and enhance the performance. An in situ supply of heat through oxidative steam reforming is also suggested. The deactivated catalyst is regenerated and recirculated back to the reformer. The CO_2-rich stream from the efficient fast fluidized membrane steam reformer is used in a reactor−regenerator dry reforming subsystem, and additional syngas is produced. A reliable reaction engineering model is utilized to investigate this novel configuration. A comparison between the predicted performance of the fast fluidized-bed reformer and the industrial data for a fixed bed as well as the pilot-plant data of the bubbling fluidized-bed configurations investigated earlier shows that the fast fluidized bed is more efficient and productive.

Introduction

Hydrogen represents one of the most promising clean fuels for the future. Hydrogen production from sources other than fossil fuels is still only in its early stages of development, and steam reforming of natural gas presently represents the principal commercial route to hydrogen production.[1] The present fixed-bed steam-reforming technology suffers from a number of inherent limitations, which result in oversized units and inefficient operation. Hence, the current reforming technologies lead to the production of hydrogen at prices (per kJ) that are 50−70% more than the highly polluting hydrocarbon fuels. The current state of affairs calls for advancing the state of the art by developing a new technology that can handle a wide variety of feedstocks, overcomes thermodynamic and other limitations, and delivers pure hydrogen economically with minimum impact on the environment.

The kinetics of the steam reforming of methane on a Ni-based catalyst were extensively investigated by Xu and Froment.[2] Elnashaie et al.[3] showed that the kinetic rate equations of Xu and Froment[2] predict well both positive and negative effective reaction orders[4,5] with respect to steam; i.e., the rate of the reaction actually has a nonmonotonic dependence on steam. The reaction is described by

$$CH_4 + H_2O \rightleftharpoons CO + 3H_2 \qquad \Delta H° = 206 \text{ kJ/mol} \quad (1)$$

$$CO + H_2O \rightleftharpoons CO_2 + H_2 \qquad \Delta H° = -41 \text{ kJ/mol} \quad (2)$$

$$CH_4 + 2H_2O \rightleftharpoons CO_2 + 4H_2 \qquad \Delta H° = 165 \text{ kJ/mol} \quad (3)$$

* Corresponding author. E-mail: ppradeep@eng.auburn.edu. Phone: 1-334-8442051. Fax: 1-334-8442063.

The classical (first-generation) process for steam reforming consists of hundreds of parallel catalyst tubes of relatively small diameter surrounded by a very large furnace. Heat for the highly endothermic reactions is supplied by radiant gas burners in a top- or side-fired configuration. The reaction is carried out at temperatures in the range of 800−1000 K and at pressures in the range of 20−25 bar. Relatively large Ni/Al_2O_3 catalyst particles are used to avoid excessive pressure drop through the reformer. This configuration suffers from limitations that can be summarized as below:

(1) *Diffusional limitations*: The large size of the catalyst pellets causes intraparticle diffusion limitations, reducing the apparent catalyst activity, and hence effectiveness factors as low as 10^{-2}−10^{-3} are observed.[6]

(2) *Thermodynamic limitations*: The reversible nature of the reactions limits the conversion to that of the thermodynamic equilibrium and necessitates the use of elevated temperatures to achieve acceptable levels of conversion and reaction rate.

(3) *Catalyst deactivation*: Carbon formation increases with the increase in the temperature and decreases with the increase in the steam-to-hydrocarbon ratio.

Elnashaie and Adris[7] first proposed the use of a fluidized-bed steam reformer using a powdered catalyst, making $\eta = 1.0$. This second-generation reformer underwent further remarkable enhancements in performance,[8] by the use of composite hydrogen permselective membranes to "break" the thermodynamic barrier of equilibrium and push the reaction toward higher conversions, even at lower temperatures. Adris[9] and Adris et al.[10−12] further studied and validated the concept of the fluidized-bed membrane reformer (FBMR) by building a pilot plant and undertaking experimental and modeling studies of the system. To improve the thermal efficiency of the reactor, some oxygen can also be

10.1021/ie0202928 CCC: $22.00
Published on Web 11/13/2002

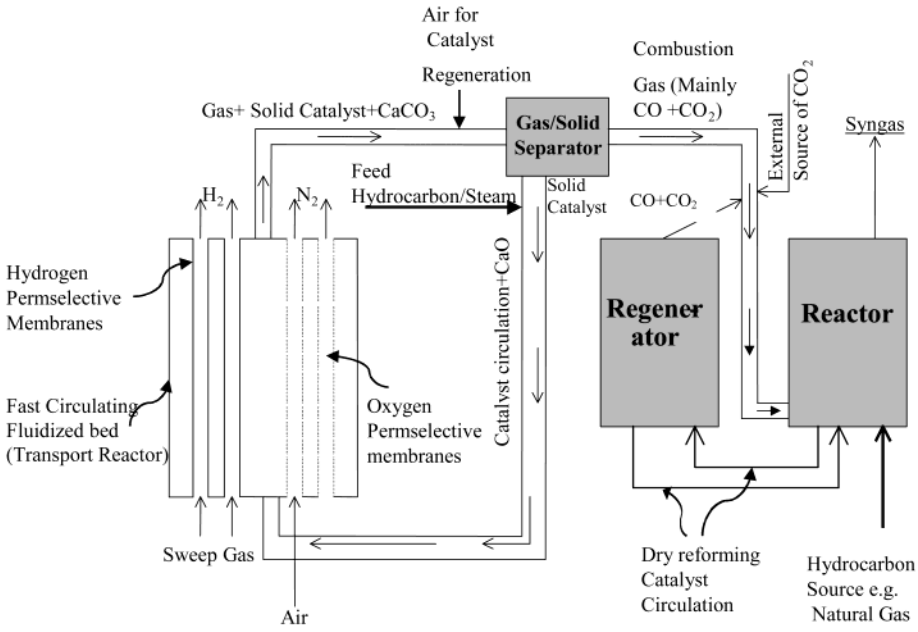

Figure 1. Schematic diagram of the proposed novel configuration.

introduced into the reactor. Thus, the exothermic combustion and partial oxidation reactions generate the heat required for the endothermic reforming reaction. Roy et al.[13] found that autothermal conditions could be reached and maintained through the addition of oxygen to the FBMR.

This configuration, although very efficient, still suffers from limitations with regard to the flow rate that can be used in a bubbling fluidized bed. Furthermore, it is not suitable for higher hydrocarbons because it does not have any provisions for handling the excessive carbon formation associated with higher hydrocarbons. Our present and future work will suggest several improvements to this second-generation configuration and introduce the third-generation reformer, which is more advanced, efficient, productive, and flexible than the previous two generations.

Main Features of the Present Novel Configuration (Third-Generation Reformer)

Figure 1 shows a complete schematic diagram of the suggested novel configuration. The salient features of the configuration are presented below:

Circulating Fluidized-Bed Reformer. Powdered catalyst particles and selective membranes are used to break the diffusion and thermodynamic barriers, respectively. The use of powdered catalysts makes the intraparticle diffusion resistance negligible, and hence $\eta = 1.0$. Also, any change in the particle size during fluidization will not affect the fact that $\eta = 1.0$. However, to break the hydrodynamic limitation "born" after the diffusion and equilibrium limitations are broken, a circulating fast fluidized bed [14−16] with much higher flow rates than those used in the bubbling fluidized beds is proposed for the reforming reactor. Lim et al.[14] have reviewed the developments in the field of gas−solid fluidization, and they have enumerated several advantages of circulating fluidized-bed reactors over the conventional bubbling and turbulent fluidized beds, including a favorable gas−solid contacting efficiency, a more uniform distribution of solids due to reduced gas bypassing, reduced gas and solid backmixing, and higher gas throughput. These advantages make a circulating fluidized-bed system very useful for reactions with short contact time, reactions with rapidly deactivating catalyst, reactions requiring considerable addition of heat where solids can be used as heat carriers and gas−solid reactions where gas−particle contact efficiency is essential. Kunii and Levenspiel[15] have developed a flow and contacting model to represent a circulating fluidized bed. Their paper gives a rough estimate of the solid fraction in the different contacting regimes, which can range from 0.2 in the fast fluidization regime to 0.01 in the pneumatic conveying regime.

Hydrogen Permselective Membranes. An integral part of this novel configuration is the composite hydrogen permselective membranes immersed vertically in the fast fluidized bed for removing hydrogen from the catalytic reforming bed. A sweep gas such as steam may be used on the membrane side to carry away the permeated hydrogen. It can be subsequently separated from the permeated hydrogen by simply condensing it. Other special purpose configurations are also possible wherein a catalytic hydrogenation reaction is carried out in the membrane side.[17] Hydrogen-permeable metal membranes made of palladium and its alloys are the most widely studied among the hydrogen permselective membranes because of their high hydrogen permeability, selectivity, and chemical compatibility with many hydrocarbon-containing gas streams. Inorganic membranes can be classified into two groups from the viewpoint of the raw material: ceramic membranes and metal membranes. Recent research efforts are generally focused on developing composite metal membranes consisting of a relatively thin palladium coating on hydrogen-permeable base metals or microporous/mesoporous ceramic membranes. Porous glass, alumina, and stainless steel have been selected as the support in most cases.[18−21] Porous stainless steel has been in the focus because of its mechanical durability, with its thermal expansion coefficient being close to that of palladium, in addition to its ease for gas sealing.[22] Coating the membrane with palladium on the sweep gas side will avoid attrition of the active layer by the catalyst particles. Several studies have been made about the use

of Pd membranes to shift the equilibrium of steam reforming and de-hydrogenation reactions to obtain a higher conversion than that dictated by equilibrium.[18,22−26]

Carbon Dioxide Acceptor. In addition to hydrogen removal, calcium oxide (lime) can be used as an acceptor to shift the equilibrium toward a higher conversion of methane and a higher yield of hydrogen. The reaction between lime and carbon dioxide is exothermic, and it also provides some of the heat required for the reforming reactions.[27−29] It will also decrease CO emission. The calcium carbonate thus formed will be regenerated because of the heat released by catalyst regeneration in the regenerator section.

$$CaO(s) + CO_2(g) \rightleftharpoons CaCO_3(s) \qquad \Delta H° = -178 \text{ kJ/mol} \quad (4)$$

$$CaCO_3(s) \rightleftharpoons CaO(s) + CO_2(g) \qquad \Delta H° = 178 \text{ kJ/mol} \quad (5)$$

Heat Addition. As seen earlier, a fixed-bed reformer requires a supply of heat through a huge furnace. The present novel configuration should eliminate the need for the furnace through the use of partial and complete oxidation of the feed as well as the heat generated from the regeneration of catalyst to supply the required heat. Direct in situ burning of the hydrocarbon is an effective way of delivering the heat required for the reactions as shown by Roy et al.,[13] but it is not the optimal technique as far as hydrogen productivity is concerned. As seen from the reactions (6) and (7), complete oxidation of the hydrocarbon produces carbon dioxide and water, thus consuming a part of the feed hydrocarbon without producing any hydrogen, whereas the partial oxidation or oxidative steam-reforming reaction has some productivity of hydrogen, although significantly lower than the main reforming reaction itself.

$$CH_4 + 2O_2 \rightarrow CO_2 + 2H_2O \qquad \Delta H° = -802 \text{ kJ/mol} \quad (6)$$

$$CH_4 + 0.5O_2 \rightleftharpoons CO + 2H_2 \qquad \Delta H° = -36 \text{ kJ/mol} \quad (7)$$

However, it must be noted that the reactions (6) and (7), though both exothermic, vary considerably in their exothermicities. Though reaction (6) does not produce any hydrogen, it is much more exothermic than reaction (7). Hence, the optimal approach would be to have a balance between the reactions in order to have the highest possible productivity of hydrogen while at the same time producing enough heat through the oxidation reactions to maintain the autothermal operation of the reactor. A part of the literature supports the theory that the catalytic partial oxidation reaction occurs as a result of complete oxidation of a portion of the methane feed followed by steam and dry reforming of the remaining methane.[30−32] Some researchers propose a direct oxidation mechanism involving dissociation of methane into carbon and hydrogen on the surface of the catalyst followed by other surface reactions between the adsorbed species for the formation of the final products.[33−35]

Oxygen-Permeable Membranes. The present novel reactor configuration will use oxygen-permeable membranes for supplying oxygen to the reactor for the oxidation and oxidative reforming reactions. The distribution of oxygen along the length of the reactor will improve the selectivity toward the oxidative reforming reaction, so that the optimum combination between the oxidative reforming and complete combustion and the other reforming reactions may be obtained. Further, the use of air on the O_2-permeable membrane side would do away with the need for external separation of oxygen from air, in addition to the production of pure nitrogen as an additional product. Jin et al.,[36] Ritchie et al.,[37] and Tsai et al.[38] have studied the use of dense perovskite membrane reactors for the partial oxidation of methane to syngas.

Catalyst Regeneration for the Membrane Steam Reformer. Coke formation on the catalyst causes deactivation of the catalyst.[39,40] The deactivated catalyst exiting the reformer is separated from the gases exiting the reactor using a gas−solid separator and recirculated to the reformer. The residence time within this recycle tube is used to burn off the carbon deposited using hot air and thus regenerate the catalyst. The burning of the deposited carbon being an exothermic reaction, it will bring about an increase in the temperature of the catalyst itself. The high temperature of the regenerated catalyst will also be useful for providing some of the heat for the reforming reaction.

CO_2 Sequestration Using a Novel Reactor−Regenerator Dry Reformer. Because of the efficient removal of hydrogen from the reactor and the in situ combustion and/or partial oxidation of the hydrocarbon feed in the reactor, the gases exiting the reactor side of the reformer will be relatively poor in H_2 and rich in CO_2. To avoid contributing to global warming by releasing the CO_2-rich gases to the atmosphere and at the same time making good use of the CO_2 formed, it can be sequestered by using it together with a suitable hydrocarbon in a dry reforming process.

$$CH_4 + CO_2 \rightleftharpoons 2CO + 2H_2 \qquad \Delta H° = 247 \text{ kJ/mol} \quad (8)$$

The dry reforming process produces a CO-rich syngas, which can be used as a feedstock for producing several chemicals. The dry reforming process classically suffers from fast deposition of carbon on the catalyst, preventing continuous operation. A novel promising approach is to use a fluidized-bed reactor−regenerator system (similar, in principle, to the FCC units in petroleum refining) that utilizes the carbon formed on the catalyst in the reactor to supply the heat necessary for the endothermic dry reforming reaction through the regeneration of catalyst in the regenerator and recycling the hot regenerated catalyst to the reactor. The CO_2 resulting from the carbon burning in the regenerator of the circulating bed reformer can also be recycled to the CO_2 reformer reactor. This reactor−regenerator unit can also be used independently as a stand-alone unit for pollution abatement of excessive CO_2 production from different sources.

Model Development

In the present paper, introductory modeling studies are carried out on the reactor section alone of the circulating fast fluidized-bed reformer. The fast fluidized-bed reformer is modeled as a plug-flow reactor with cocurrent flow in the reactor and membrane (sweep gas) sides. Ideal gas laws are used to calculate the partial pressures on the reactor and the membrane sides. The

Table 1. Parameters in the Rate Equations[5]

$k_1 = 9.49 \times 10^{16} \exp(-28879.0/T)$
$k_2 = 4.39 \times 10^{4} \exp(-8074.3/T)$
$k_3 = 2.29 \times 10^{16} \exp(-29336.0/T)$
$K_{CH_4} = 6.65 \times 10^{-6} \exp(4604.28/T)$
$K_{H_2O} = 1.77 \times 10^{3} \exp(-10666.35/T)$
$K_{H_2} = 6.12 \times 10^{-11} \exp(9971.13/T)$
$K_{CO} = 8.23 \times 10^{-7} \exp(8497.71/T)$
$K_1 = 10266.76 \exp[(26830/T) + 30.11]$
$K_2 = \exp[(4400.0/T) - 4.036]$

cases with and without hydrogen selective membranes are considered and are compared with industrial fixed-bed reformers and also bubbling fluidized-bed reformers with and without hydrogen selective membranes. The model results reinforce the idea of breaking the thermodynamic limitations of the reforming reactions and also introduce the advantages associated with the breaking of the hydrodynamic limitations of bubbling fluidized-bed steam reformers (BFBSRs). The oxidative steam reforming, natural gas combustion, reaction of CaO with CO_2, and dry reforming are not included in this paper.

Kinetic Rate Equations for Methane Steam Reforming. The rate expressions proposed by Xu and Froment[2] and analyzed in some detail by Elnashaie et al.[5] are used in the present study. The three main reactions along with their corresponding rate equations are given below, and the values of the kinetic parameters are given in Table 1.

$$CH_4 + H_2O \rightleftharpoons CO + 3H_2$$

$$r_1 = \frac{k_1}{p_{H_2}^{2.5}}\left[p_{CH_4}p_{H_2O} - \frac{p_{H_2}^{3}p_{CO}}{K_1}\right]/\mathrm{DEN}^2 \qquad (9)$$

$$CO + H_2O \rightleftharpoons CO_2 + H_2$$

$$r_2 = \frac{k_2}{p_{H_2}}\left[p_{CO}p_{H_2O} - \frac{p_{H_2}p_{CO}}{K_2}\right]/\mathrm{DEN}^2 \qquad (10)$$

$$CH_4 + 2H_2O \rightleftharpoons CO_2 + 4H_2$$

$$r_3 = \frac{k_3}{p_{H_2}^{3.5}}\left[p_{CH_4}p_{H_2O}^{2} - \frac{p_{H_2}^{4}p_{CO_2}}{K_1K_2}\right]/\mathrm{DEN}^2 \qquad (11)$$

where

$$\mathrm{DEN} = 1 + K_{CO}p_{CO} + K_{H_2}p_{H_2} + K_{CH_4}p_{CH_4} + K_{H_2O}p_{H_2O}/p_{H_2}$$

Hydrogen-Permeable Membrane. For commercially available palladium-based membranes, the rate of proton and electron diffusion through the palladium lattice is the limiting factor.[41] Under these conditions, thermodynamic equilibrium will be established between the hydrogen molecules in the gas phase and the atoms dissolved at the interface. Because the hydrogen concentration at the interface is proportional to the square root of the hydrogen pressure according to Sievert's law, the hydrogen flux (kmol·h^{-1}·m^{-2}) can be expressed as

$$J_{H_2\ \mathrm{removal}} = \frac{Q_0}{\delta}\exp\left(\frac{-E_a}{RT}\right)(p_{H_2,r}^{n} - p_{H_2,m}^{n}) \qquad (12)$$

where δ is the membrane thickness and the superscript m indicates the membrane side (sweep gas side). The dependence factor of the hydrogen flux on the partial pressure of hydrogen (n) sometimes deviates from 0.5. A value of n greater than 0.5 may result when surface processes influence the permeation rate or when Sievert's law is not strictly followed. In fact, n may also depend on the temperature because it is influenced by solubility and the relative rates of surface processes and bulk diffusion, all of which depend on the temperature.[18] A couple of the membranes about which data are available in the literature are considered in the present study. The data used for finding the permeation flux are given in Table 2. For membrane 1, $Q_0 = Q_0'\rho_m$, and for membranes 2 and 3, $Q_0 = Q_0'$.

Model Assumptions. The following simplifying assumptions are included in the model derivation:

(1) All parts of the system are at steady state.

(2) The reformer gas and catalyst are in plug flow and are flowing through the reformer at the same speed.

(3) There is negligible axial mixing and complete radial mixing.

(4) The volume fraction of the solid catalyst particles remains constant along the length of the reactor.

(5) The membrane is completely permselective to hydrogen and is in thermal equilibrium with the reformer gases.

(6) Pressure is constant along the length of the reactor.

Model Equations. Mass balance involves five components, viz., CH_4, H_2O, CO, CO_2, and H_2. Thus, there are five mass balance equations for the reactor side and one for the membrane side. The partial pressures involved are calculated using the ideal gas equation. An energy balance equation is also required for the nonisothermal cases.

$$\mathrm{d}F_i/\mathrm{d}l = \rho_c A_c(1-\epsilon)R_i - Q_i \qquad (13)$$

$$\sum_i F_i\frac{\mathrm{d}H_i}{\mathrm{d}l} = A_c\rho_c(1-\epsilon)\sum_j r_j(-\Delta H_j) + Q \qquad (14)$$

In the mass balance equations, $R_i = 0$ for the mass balances for hydrogen in the hydrogen-permeable membrane side. $Q_i = 0$ for all components, except hydrogen for which Q_i is the corresponding molar permeation term depending on the type of membrane used. Also, Q_i is positive for the reactor side and negative for the membrane side. For a supported dense Pd membrane, the hydrogen permeation term is given below. Values of the parameters from Collins and Way[18] and Shu et al.[41] have been used in the present study.

$$Q_{H_2} = Q_0\left(\frac{\pi d_m n_t}{\delta}\right)\exp\left(\frac{-E_a}{RT}\right)(p_{H_2,r}^{n} - p_{H_2,m}^{n}) \qquad (15)$$

The methane and steam conversions have the usual definitions. The total hydrogen yield is calculated as the total amount of hydrogen produced (i.e., molar flow rate of hydrogen in the reactor side as well as the membrane side) per mole of methane introduced. The value of "hydrogen yield per cubic meter of reactor" has been

Table 2. Data Used for the Hydrogen-Permeable Membranes

	membrane description	Q_0'	E_a (kJ·mol^{-1})	n	ref
1	Pd−Ag on SS support (thickness = 20 μm)	1.776×10^{-3} (m^2·kPa$^{-0.5}$·h^{-1})	15.7	0.5	Shu and Grandjean[42]
2	Pd on ceramic support (thickness = 17 μm)	9.9714×10^{-6} (kmol·m^{-1}·kPa$^{-0.573}$·h^{-1})	14.45	0.573	Collins and Way[18]
3	Pd on ceramic support (thickness = 11.4 μm)	3.2049×10^{-6} (kmol·m^{-1}·kPa$^{-0.58}$·h^{-1})	8.88	0.58	Collins and Way[18]

Table 3. Data of an Industrial Top-Fired Fixed-Bed Steam Reformer[6]

Reformer Tubes	
heated length of the reformer tube (m)	13.7
inside diameter of the reformer tube (m)	0.097
catalyst bulk density (kg/m^3)	1362.0
Outlet Conditions	
process gas temperature (K)	1130
conversion of CH_4	0.8527
Inlet Conditions per Tube	
process gas flow rate (methane equivalent) (kmol/h)	3.953
temperature (K)	760.0
pressure (kPa)	2837
steam-to-methane ratio	3.5610
hydrogen-to-methane ratio	0.2432
carbon dioxide-to-methane ratio	0.1209
nitrogen-to-methane ratio	0.0204
Composition (mol %)	
CH_4	20.22
H_2O	72.00
H_2	4.92
CO_2	2.44
N_2	0.42

used as an estimation of the efficiency of the reactor when comparing reactors.

$$Y_{H_2} = \frac{F_{H_2,m} + F_{H_2,r} - F^0_{H_2}}{F^0_{CH_4}} \tag{16}$$

In this paper the following values have been used unless otherwise stated: the cross-sectional area (A_c) of the reactor available for flow of reactants is 75.12 cm^2, the length of the reactor is 2 m, the diameter of the membrane tubes (d_m) is 2 mm, the number of hydrogen-permeable membrane tubes (n_t) is 500, the reactor pressure is 21.7 atm, and the pressure on the hydrogen-permeable membrane side is 1 atm.

Solution of the Model Equations. The model equations are highly nonlinear initial value ordinary differential equations (ODEs) that can be solved using a suitable integration subroutine such as the IVPAG subroutine in the IMSL library. The subroutine uses Gear's stiff methods with automatic step size adjustment. The feed composition and flow rate of an industrial fixed-bed reactor[6] was used as initial conditions (Table 3) unless otherwise stated. It should be noted that the nonzero flow rate of H_2 in the feed circumvents the problem of the infinite rate of reaction at zero hydrogen partial pressure as predicted by the kinetic rate equations.

Hydrodynamics. To check the hydrodynamic regime at which the reactor is operating, the method described by Kunii and Levenspiel[15] is used. The dimensionless particle size and dimensionless gas velocity (eqs 17 and 18) are first found using the physical properties of the gas mixture and a particle size of 186 μm (which is actually the average diameter of the catalyst particles used by Adris[9] for the successful pilot plant-tests of the BFBSR). The superficial gas velocities in the reactor are obtained using ideal gas law from the molar flow rates obtained from the solution of the model.

$$d_p^* = d_p\left[\frac{\rho_g(\rho_s - \rho_g)g}{\mu^2}\right]^{1/3} \tag{17}$$

$$u^* = u\left[\frac{\rho_g^{\,2}}{\rho_g(\rho_s - \rho_g)g}\right]^{1/3} \tag{18}$$

The generalized map of gas−solid contacting as reported in Lim et al.[14] and also in Kunii and Levenspiel[15] can then be used to check the regime of operation of the reactor. In all of the results of the present investigation, the above procedure was followed to ensure that the reactor was in either the fast fluidization or the pneumatic transport regime.

Results and Discussion

Isothermal Case. It was found that the reaction reaches maximum conversion at an extremely small value for the length of the reactor. This can be seen in Figure 2a (no membrane case), which shows the conversion of methane along the length of a reactor without a Pd membrane at isothermal conditions (T = 1000 K). The equilibrium conversion is reached in less than 10 cm of length of the reactor because of the drastic increase in the effectiveness factor from 10^{-2} to 10^{-3} in the fixed bed to 1 in the fluidized bed. Here, because a fast fluidized bed is being used, the flow rates (and hence the hydrogen productivity) can actually be higher than those used in this example. However, this case clearly shows the effect of the fast fluidization regime on the conversion of methane.

Further improvement can be brought about by the use of a membrane, which breaks the thermodynamic barrier and makes the reaction proceed toward higher conversions of methane as can be seen in Figure 2a. Figure 2a shows the comparison between a membrane reactor and another one without the membrane. In the presence of the membrane, the reaction proceeds to almost complete conversion of methane in about 2 m of reactor length. This is a huge improvement over the 13.72 m length that was required for an 85% conversion of methane in the fixed-bed industrial data that had an exit temperature of 1130 K.[6] Two different membranes (thicknesses of 17 and 11.4 μm) studied by Collins and Way[18] were used in the study and found to give almost similar performances. Along the length of the reactor, as the reactants are consumed and hydrogen gets selectively permeated to the membrane side, the driving force for hydrogen permeation becomes smaller and smaller. However, as long as there is a difference in the partial pressures of hydrogen in the reaction and permeation side (Figure 2b), hydrogen will continuously be removed from the reactor and the equilibrium will be shifted toward higher production of hydrogen.

Temperature affects not only the reaction rate within the reactor but also the flux of hydrogen through the

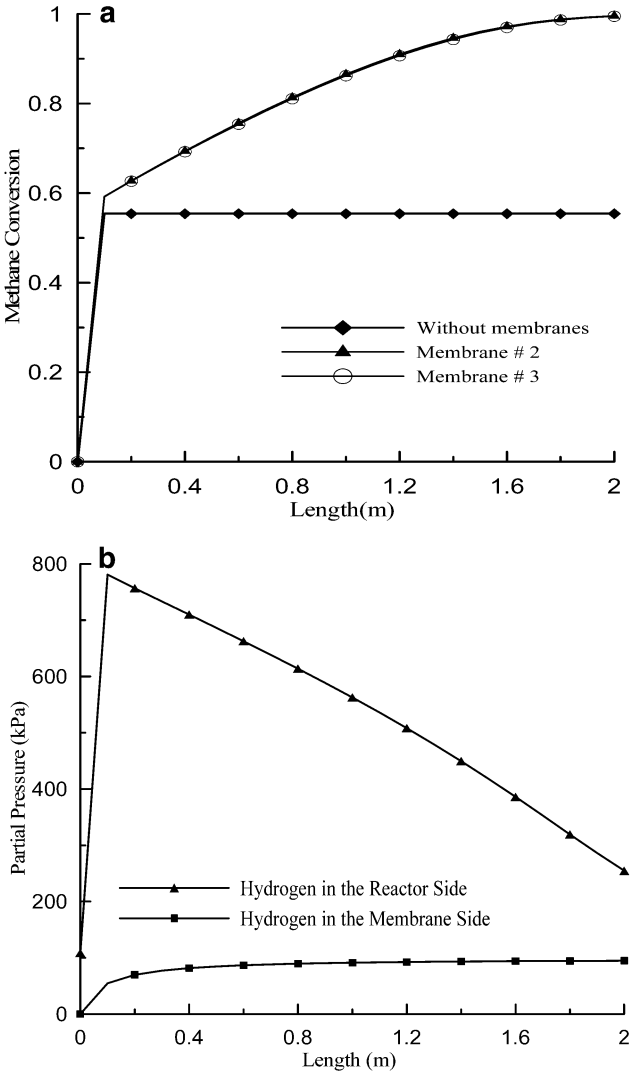

Figure 2. (a) Conversion of methane as a function of the length of the reactor for the isothermal case (T = 1000 K). (b) Partial pressure of hydrogen as a function of the length of the reactor.

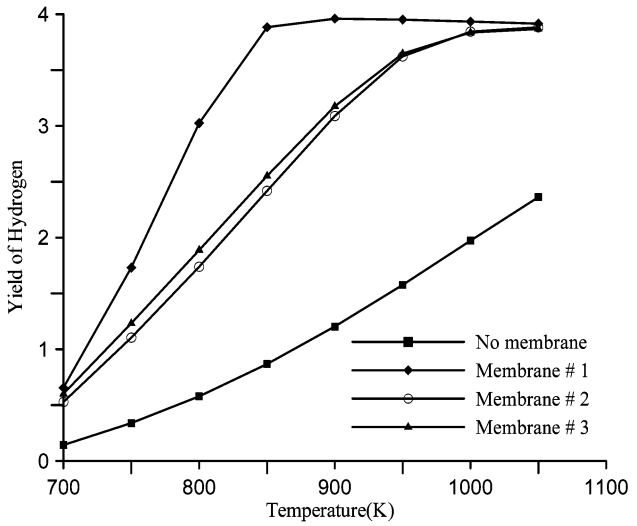

Figure 3. Effect of the temperature. Yield of hydrogen vs temperature.

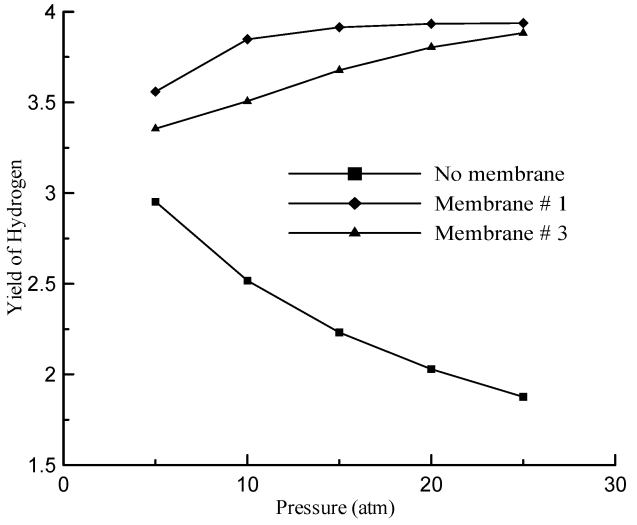

Figure 4. Effect of the pressure. Yield of hydrogen vs pressure.

membrane. Thus, significantly higher conversions and yields can be obtained in a fast fluidized bed using hydrogen permselective membranes as compared to one without the membranes (see Figure 3), and the improvement is greater at higher temperatures. The hydrogen yield starts to level off toward the maximum value of 4 as the rate of reaction and the hydrogen permeation start to cause complete conversion. If the temperature is increased further, it will manifest itself not through an increase in the hydrogen yield but through a decrease in the length of the reactor needed to achieve complete conversion.

Figure 4 shows that the methane conversion in the membrane reactor can increase with an increase in the pressure. The reforming reaction involves an increase in the number of moles and hence should show a lower conversion at higher pressures. However, in the presence of the membrane, higher reactor pressure would result in a greater driving force for permeation of hydrogen. Hence, the conversion in a membrane reactor is actually the net result of these two effects that tend to affect the conversion in opposing ways. Another factor to be noted about operation at higher pressures is that, at higher pressures, a greater molar flow rate can be passed for a particular velocity, thus leading to higher production of hydrogen. In order for the reactor to be operated at higher pressures, it is necessary for the membrane to have sufficient mechanical strength. The 11.4 μm thick membrane made by Collins and Way[18] is reported to have been tested at pressure differences of up to 1500 kPa. Collins and Way[18] have also tested other membranes at pressure differences of up to 2330 kPa, but permeability constants are not available for those.

The effect of the permeation area was studied using the Collins and Way[18] 11.4 μm membrane. The permeation rate equation suggests that the amount of hydrogen permeated is directly proportional to the membrane surface area, so increasing the membrane surface area by increasing the number of membrane tubes in the reactor will enable more of the hydrogen to be removed by the membranes. At a particular temperature, an increase in the number of membrane tubes will thus result in either a higher hydrogen yield for a given length of reactor or a lower reactor length requirement for a particular hydrogen yield. Figure 5 shows the effect of increasing the number of membrane tubes at a constant tube diameter and length, at different temperatures. The effect of the membrane surface area was investigated at a constant reactor length and cross-sectional area in order to maintain uniformity. The effect of increasing the membrane surface area is not

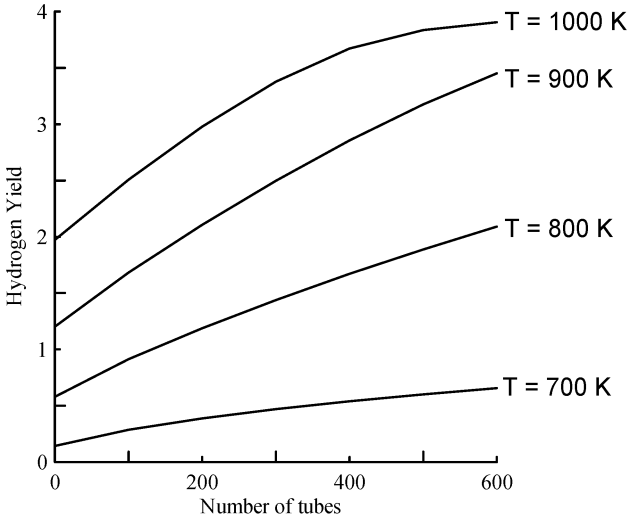

Figure 5. Effect of the permeation area (number of membrane tubes).

appreciable at lower temperatures because of the low rate of reaction and equilibrium conversion. A steeper increase in the yield is observed for the case with higher temperature. This is due to the combined effects of a faster rate of steam-reforming reaction (which increases the hydrogen partial pressure in the reactor and thus increases permeation) as well as an increase in the hydrogen permeation area. The permeation rate shows an Arrhenius-type dependence on the temperature. Hence, increasing the membrane surface area will have a stronger effect at a higher temperature. At higher temperatures (e.g., 1000 K), the hydrogen yield starts to approach its maximum value of 4 as the number of membrane tubes is increased to about 600 (i.e., 7.5 m^2 of membrane surface area) and above.

Nonisothermal Case. For an adiabatic reactor ($Q = 0$), there is a sharp decrease in the temperature in a small region at the beginning of the reactor for cases with and without membranes (see Figure 6a). Most of the reaction occurs in this region where the concentration of the reactants is high. For the reactor with the membrane (parameters for membrane no. 3 in Table 2 are used in this case), some amount of reaction also occurs after that region because of the effect of the membrane, leading to a drop in temperature. Thus, higher methane conversions are attainable even at lower temperature.

The selection of an optimum temperature and heat profile and the mode of introduction of heat is a more involved process that needs further study. It is assumed here that a constant amount of heat (Q, $kJ \cdot h^{-1} \cdot m^{-1}$) is being introduced along the length of the reactor. Even with this rather simplistic assumption, a variety of possible temperature profiles exist, depending on the operating conditions, feed temperature, and heat supplied. Parts a and b of Figure 6 also show the effect of the membrane when some heat is input to the reactor and for an inlet temperature of 900 K. The temperature profile is steeper and the outlet temperature is higher for the case without membrane. In the absence of the membrane, even though a part of the supplied heat is utilized for carrying the reaction forward, the heat supplied is used mainly to raise the temperature of the reactor gases. However, in the presence of the membrane, the equilibrium is pushed forward and more of the heat is utilized for carrying out the reaction itself.

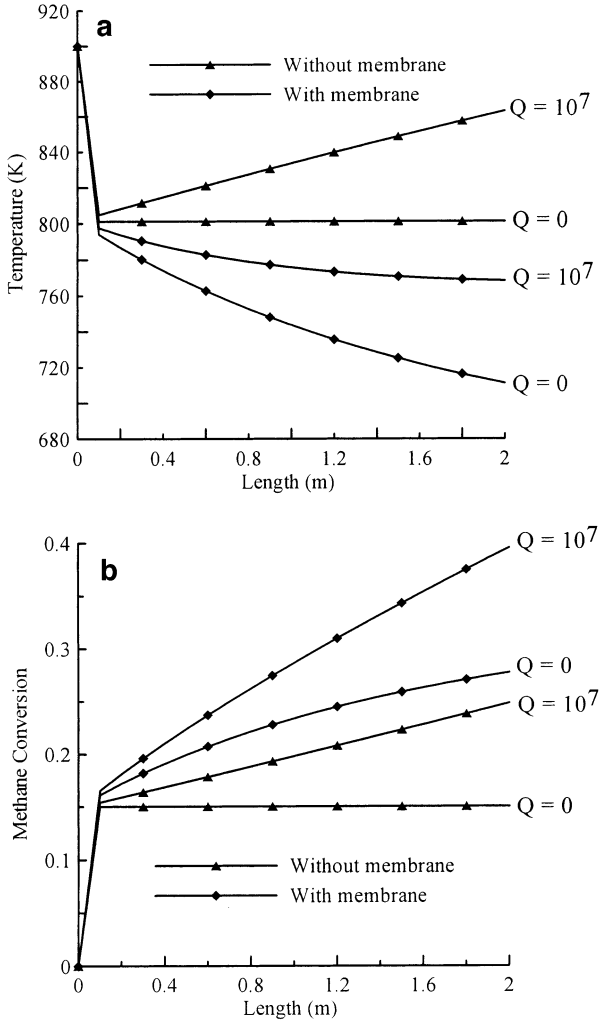

Figure 6. (a) Nonisothermal adiabatic case: temperature vs length of the reactor. (b) Nonisothermal adiabatic case: methane conversion vs length of the reactor for the case in part a.

Table 4. Comparison between the Fixed-Bed Data and the Model Predictions for the FFMSR

	fixed bed[6]	FFMSR[a]		
		case I	case II	case III
exit methane conversion	0.8527	0.8675	0.913	0.9375
exit steam conversion	0.3405	0.3226	0.3524	0.3721
total hydrogen yield (per mole of methane introduced)	2.812	2.884	3.081	3.200
methane feed rate (mol/h)	3953	3953	3953	3953
process gas exit temperature (K)	1130	1130.57	1130.79	1130
pressure (kPa)	2200	2200	2200	2200
length (m)	13.72	0.2	2	2
total reactor volume (m^3)	0.1031	0.0018	0.018	0.018
membrane diameter (mm)		9.78	9.78	9.78
membrane surface area (m^2)		0.123	1.229	1.229
hydrogen yield per cubic meter of reactor	27.27	1602.2	171.2	177.8

[a] Using parameters for the Collins and Way[18] membrane (11.4 μm).

A comparison is performed between the fast fluidized membrane steam reformer (FFMSR) and the industrial fixed-bed reactor data and the bubbling fluidized-bed pilot-plant data. Table 4 presents a comparison between the results from the model for the FFMSR developed in this paper and the data from an industrial fixed-bed

Table 5. Comparison between the BFBSR Model Data and FFSR Model Data

	BFBSR[7]	FFSR
methane feed rate (kmol/h)	709.28	709.28
feed temperature (K)	1200	1200
process gas exit temperature (K)	1182.8	1182.4
pressure (kPa)	2010	2010
length (m)	0.40	2.0
diameter (m)	4.022	0.0978
reactor volume (m^3)	3.81	0.015
catalyst dilution factor	0.224	0.224
exit methane conversion	0.913	0.966
exit steam conversion	0.293	0.287

reactor.[6] The feed conditions, operating pressure, and diameter of the reactor tube are the same for both reactors. Even though the molar feed flow rate and the cross-sectional area are the same for both reactors, the difference in the size of the catalyst particle makes the FFMSR operate in the fast fluidization regime. The comparison again shows the effect of overcoming not only the diffusion resistance of the catalyst pellets in the fixed bed but also the breaking of the thermodynamic barrier of equilibrium by the use of the palladium membrane. A key figure to note is the hydrogen yield per cubic meter of the reactor (i.e., moles of hydrogen produced per hour per cubic meter of the reactor per mole of methane introduced), which is an important indication of the efficiency of the reactor. It normalizes the hydrogen produced with both the feed rate and the size of the reactor, allowing for comparison of different types of reactors having different scales of operation. In all of the cases, the temperature profile was adjusted using the heat input in such a way that the outlet temperature is very close to that of the fixed bed. In case I, the methane conversion is very close to that of the fixed bed but still the yield of hydrogen is higher for the FFMSR. This can be attributed to the effect of the membrane. Furthermore, this can be brought about at a fraction of the volume required for a fixed bed. Case II shows another sample run for a greater reactor volume than case I. The greater length should make it easier for us to supply the heat for the reaction. Case III is an isothermal case at the outlet temperature of the fixed-bed reactor.

Table 5 shows a comparison between the model results for a BFBSR[7] (without H_2 permeable membranes) and the model results for the fast fluidized steam reformer (FFSR). The comparison was done for the same feed rate and compositions. The bubbling fluidized bed acts as a well-mixed reactor, but its performance is enhanced because of the effect of the removal of the reaction products by the bubbles, which act as natural membranes. The model for the BFBSR contained a dilution factor for the catalyst, to obtain a practically feasible value for the volume of the reactor, which would otherwise be very small because of the high effectiveness factor. The same dilution factor is used in the model of the FFSR for the sake of this comparison only. The heat input to the FFSR was adjusted in such a way as to obtain the same process gas temperature as the BFBSR. It is seen from the comparison table that a higher conversion can be obtained for a smaller reactor volume. This is because of the efficiency of the fast fluidization regime, which is almost plug flow in nature, while the bubbling fluidized bed is like a well-mixed reactor but with the bubbles acting as natural membranes and enhancing the performance.

Table 6. Comparison between the BFBSR and the Model Predictions for an Isothermal FFMSR

		FFMSR[a]		
	BFBSR[9]	case I	case II	case III
exit methane conversion	0.419	0.309	0.398	0.300
exit steam conversion	0.2	0.162	0.201	0.156
total hydrogen yield (per mole of methane introduced)	1.515	1.194	1.511	1.156
methane feed rate (mol/h)	41.2	1977	1977	1977
process gas exit temperature (K)	814	814	850	814
pressure (kPa)	640	640	640	640
length (m)	1.14	1.88	1.88	0.188
diameter (mm)	97	97	97	97
reactor volume (m^3)	0.0139	0.014	0.014	0.0014
membrane diameter (mm)	4.7	4.7	4.7	4.7
membrane surface area (m^2)	0.0975	0.111	0.111	0.111
hydrogen yield per cubic meter of reactor	109	85.3	108	824.1

[a] Using parameters for the Collins and Way[18] membrane (11.4 μm).

Table 6 shows the comparison between the FFMSR and the experimental results from the pilot plant for the BFBSR[9] (with H_2 permeable membranes). This comparison represents a more challenging case because of the well-mixed nature of the fluidized bed and also the fact that the bubbles act as natural membranes and help to increase the conversion. The temperature and the concentrations in the dense phase of the bubbling fluidized bed will be the same at all points. Hence, in all of the cases of comparison, the isothermal model had been used for the FFMSR. In all of the cases, the operating pressure is the same as the BFBSR but with a higher feed flow rate to be able to operate in the fast fluidization regime. The other inlet conditions for the FFMSR were as given in Table 3. Case I is an isothermal reactor of the same volume and at the same temperature as the BFBSR. However, with lower hydrogen yield per cubic meter than that of the BFBSR. This is due, in addition to the reasons mentioned above, to the fact that the feed flow rate is much smaller than that in the FFMSR. Because the volume has been considered the same in both cases, the residence time is much higher in the BFBSR. For the same volume, one can get the same performance at just a slightly higher temperature of 850 K (case II). However, it is actually possible to obtain a conversion and yield close to that in case I in a much smaller length of the FFMSR. Also, this is what case III shows. There is a clear increase in the hydrogen yield per cubic meter of the reactor. This last case actually gives a more realistic comparison of the efficiency of the reactors. Of course, in all of the above cases the actual moles of hydrogen produced per hour will be much higher than the BFBSR because of the higher flow rate that can be used in a fast fluidized bed as compared to the BFBSR.

Conclusion

A novel reactor configuration using a recirculating FFMSR was proposed for overcoming the limitations of the fixed-bed and BFBSRs. The fluidized-bed steam reformer has a hydrogen-permeable membrane to continuously remove hydrogen and an oxygen-permeable membrane to supply oxygen into the reactor for partial oxidation reaction. The use of powdered catalyst par-

ticles overcomes the traditional diffusion limitation of the catalyst pellets. The use of hydrogen selective membranes overcomes the thermodynamic limitations of the steam-reforming reaction. Also, the use of fast fluidization overcomes the hydrodynamic limitations of a bubbling fluidized bed. A preliminary modeling and parametric study was performed on the steam reformer part alone, using plug-flow behavior and a Pd membrane to selectively remove H_2 from the reaction mixture. The results of the simulation and comparison with available data about previous generations of reformers indicate that a substantial increase in hydrogen productivity can be obtained using much smaller reactors. The configuration offers the possibility of efficient and economic production of pure hydrogen and encourages further scientific and economic investigation.

Acknowledgment

This research was supported by Auburn University through Grant 2-12085.

Nomenclature

A_c = cross-sectional area of the reactor (m^2)
d_m = diameter of the membrane tube (m)
d_p = diameter of the catalyst particle (m)
d_p^* = dimensionless measure of the particle diameter
E_a = apparent activation energy of the composite palladium membrane ($kJ \cdot mol^{-1}$)
F_i, F_i^0 = molar flow rate, molar feed flow rate of species i ($kmol \cdot h^{-1}$)
ΔH_j = heat of reaction for reaction j ($kJ \cdot mol^{-1}$)
k_1, k_3 = rate constants ($kmol \cdot kPa^{0.5} \cdot kg\ of\ catalyst^{-1} \cdot h^{-1}$)
k_2 = rate constant ($kmol \cdot kPa^{-1} \cdot kg\ of\ catalyst^{-1} \cdot h^{-1}$)
K_1 = equilibrium constant for reaction (1) (kPa)
K_2 = equilibrium constant for reaction (2)
l = distance along the reactor (m)
$p_{H_2,r}$, $p_{H_2,m}$ = hydrogen partial pressure on the reaction and membrane sides, respectively (kPa)
p_i = partial pressure of species i (kPa)
Q_0 = preexponential factor in the Arrhenius relationship ($kJ \cdot m^{-1} \cdot h^{-1} \cdot kPa^{-n}$)
$J_{H_2\ removal}$ = hydrogen flux ($kmol \cdot h^{-1} \cdot m^{-2}$)
Q = rate of heat input ($kJ \cdot h^{-1} \cdot m^{-1}$)
r_j = rate of reaction j ($kmol \cdot h^{-1} \cdot kg\ of\ catalyst^{-1}$)
R = gas constant
R_i = rate of production of species i ($kmol \cdot h^{-1} \cdot kg\ of\ catalyst^{-1}$)
T = temperature (K)
u = superficial velocity ($m \cdot s^{-1}$)
u^* = dimensionless gas velocity
X_{CH_4}, X_{H_2O} = conversion of methane and steam
Y_{H_2} = yield of hydrogen

Greek Letters

δ = thickness of the palladium membrane (m)
ϵ = void fraction
ρ_c = density of the catalyst ($kg \cdot m^{-3}$)
ρ_g = density of the reaction gases ($kg \cdot m^{-3}$)
ρ_m = molar density of the reaction gases ($kmol \cdot m^{-3}$)
μ = viscosity ($kg \cdot m^{-1} \cdot s^{-1}$)

Literature Cited

(1) Brown, L. F. A Comparative Study of Fuels for On-Board Hydrogen Production for Fuel-Cell-Powered Automobiles. *Int. J. Hydrogen Energy* **2001**, *26*, 381.

(2) Xu, J.; Froment, G. F. Methane Steam Reforming, Methanation and Water Gas Shift—I. Intrinsic Kinetics. *AIChE J.* **1989**, *35*, 88.

(3) Elnashaie, S. S. E. H.; Adris, A. M.; Al-Ubaid, A. S.; Soliman, M. A. On the Non-Monotonic Behavior of Methane Steam Reforming Kinetics. *Chem. Eng. Sci.* **1990**, *45* (2), 491.

(4) Bodrov, N. M.; Apel'Baum, L. O.; Temkin, M. I. Kinetics of the Reaction of Methane with Steam on the Surface of Nickel. *Kinet. Katal.* **1964**, *5*, 696.

(5) De Deken, J. C.; Devos, E. F.; Froment, G. F. Steam Reforming of Natural Gas. *Chem. React. Eng.—Boston. Int. Symp., 7th* **1982**, 196.

(6) Elnashaie, S. S. E. H.; Elshishini, S. S. *Modelling, Simulation and Optimization of Industrial Fixed Bed Catalytic Reactors*; Gordon and Breach Science Publishers: London, 1993.

(7) Elnashaie, S. S. E. H.; Adris, A. M. A Fluidized Bed Steam Reformer for Methane. *Proceedings of the VI International Fluidization Conference, Banff, Canada*; AIChE Publication 319; AIChE: New York, 1989.

(8) Adris, A. M.; Elnashaie, S. S. E. H.; Hughes, R. A Fluidized Bed Membrane Reactor for the Steam Reforming of Methane. *Can. J. Chem. Eng.* **1991**, *69*, 1061.

(9) Adris, A. M. A fluidized bed membrane reactor for steam reforming: experimental verification and model validation. Ph.D. Dissertation, University of British Columbia, Vancouver, Canada, 1994.

(10) Adris, A. M.; Grace, J. R.; Lim, C. J.; Elnashaie, S. S. E. H. Fluidized Bed Reaction System for Steam/Hydrocarbon Reforming to Produce Hydrogen. U.S. Patent 5,326,550, 1994.

(11) Adris, A. M.; Lim, J.; Grace, J. R. The Fluidized Bed Membrane Reactor (FBMR) System: a Pilot Scale Experimental Study. *Chem. Eng. Sci.* **1994**, *49*, 5833.

(12) Adris, A. M.; Lim, C. J.; Grace, J. R. The Fluidized Bed Membrane Reactor for Steam Methane Reforming: Model Verification and Parametric Study. *Chem. Eng. Sci.* **1997**, *52*, 1609.

(13) Roy, S.; Pruden, B. B.; Adris, A. M.; Lim, C. J.; Grace, J. R. Fluidized-bed Steam Methane Reforming with Oxygen Input. *Chem. Eng. Sci.* **1999**, *54*, 2095.

(14) Lim, K. S.; Zhu, J. X.; Grace, J. R. Hydrodynamics of Gas—Solid Fluidization. *Int J. Multiphase Flow* **1995**, *21* (Suppl.), 141.

(15) Kunii, D.; Levenspiel, O. Circulating Fluidized-Bed Reactors. *Chem. Eng. Sci.* **1997**, *52*, 2471.

(16) Kehlenbeck, R.; Yates, J.; Di Felice, R.; Hofbauer, H.; Rauch, R. Novel scaling parameter for circulating fluidized beds. *AIChE J.* **2001**, *47* (3), 582—589.

(17) Elnashaie, S. S. E. H.; Moustafa, T.; Alsoudani, T.; Elshishini, S. S. Modeling and Basic Characteristics of Novel Integrated Dehydrogenation—Hydrogenation Membrane Catalytic Reactors. *Comput. Chem. Eng.* **2000**, *24*, 1293.

(18) Colllins, J. P.; Way, J. D. Preparation And Characterization Of Composite Palladium-Ceramic Membrane. *Ind. Eng. Chem. Res.* **1993**, *32*, 3006.

(19) Yeung, K. L.; Christiansen, S. C.; Varma, A. Palladium Composite Membranes by Electroless Plating Technique. Relationships between Plating Kinetics, Film Microstructure and Membrane Performance. *J. Membr. Sci.* **1999**, *159*, 107.

(20) Prabhu, A. K.; Oyama, S. T. Highly Hydrogen Selective Membranes: Application to the Transformation of Greenhouse Gases. *J. Membr. Sci.* **2000**, *176*, 233.

(21) Wu, L.; Xu, N.; Shi, J. Preparation of a Palladium Composite Membrane by an Improved Electroless Plating Technique. *Ind. Eng. Chem. Res.* **2000**, *39*, 342.

(22) Shu, J.; Adnot, A.; Grandjean, B. P. A.; Kaliaguine, S. Structurally Stable Composite Pd—Ag Alloy Membranes: Introduction of a Diffusion Barrier. *Thin Solid Films* **1996**, *286*, 72.

(23) Barbieri, G.; Maio, F. P. D. Simulation of the Methane Steam Reforming Process in a Catalytic Pd-Membrane Reactor. *Ind. Eng. Chem. Res.* **1997**, *36*, 2121.

(24) Kikuchi, E. Membrane Reactor Application to Hydrogen Production. *Catal. Today* **2000**, *56*, 91.

(25) Kikuchi, E.; Nemoto, Y.; Kajiwara, M.; Uemiya, S.; Kojima, T. Steam Reforming of Methane in Membrane Reactors: Comparison of Electroless Plating and CVD Membranes and Catalyst Packing Modes. *Catal. Today* **2000**, *56*, 75.

(26) Prabhu, A. K.; Liu, L. G.; Lovell, S. T.; Oyama, S. T. Modeling of the Methane Reforming Reaction in Hydrogen Selective Membrane Reactors. *J. Membr. Sci.* **2000**, *177*, 83.

(27) Balasubramanian, B.; Lopez Ortiz, A.; Kaytakoglu, S.; Harrison, D. P. Hydrogen from Methane in a Single Step Process. *Chem. Eng. Sci.* **1999**, *54*, 3543.

(28) Silaban, A.; Harrison, D. P. High-Temperature capture of Carbon Dioxide: Characteristics of the Reversible Reaction Between CaO(s) and CO_2(g). *Chem Eng. Commun.* **1995**, *137*, 177.

(29) Barker, R. J. The Reversibility of the Reaction $CaCO_3 \rightleftharpoons CaO + CO_2$. *Appl. Chem. Biotechnol.* **1973**, *23*, 733.

(30) Vermeiren, W. J. M.; Blomsma, E.; Jacobs, P. A. Catalytic and Thermodynamic Approach of the Oxyreforming Reaction of Methane. *Catal. Today* **1992**, *13*, 427.

(31) Dissanayake, D.; Rosynek, M. P.; Kharas, K. C. C.; Lungsford, J. H. Partial Oxidation of Methane to Carbon Monoxide and Hydrogen over a Ni/Al_2O_3 Catalyst. *J. Catal.* **1991**, *132*, 117.

(32) De Groote, A. M.; Froment, G. F. Simulation of the Catalytic Partial Oxidation of Methane to Synthesis Gas. *Appl. Catal. A* **1996**, *138*, 245.

(33) Hickman, D. A.; Schmidt, L. D. Production of Syngas by Direct Catalytic Oxidation of Methane. *Science* **1993**, *259*, 343.

(34) Bharadwaj, S. S.; Schmidt, L. D. Catalytic Partial Oxidation of Natural Gas to Syngas. *Fuel Process. Technol.* **1995**, *42*, 109.

(35) Jin, R.; Chen, Y.; Li, W.; Cui, W.; Ji, Y.; Yu, C.; Jiang, Y. Mechanism for Catalytic Partial Oxidation of Methane to Syngas over a Ni/Al_2O_3 Catalyst. *Appl. Catal. A* **2000**, *201*, 71.

(36) Jin, W.; Gu, X.; Li, S.; Huang, P.; Xu, N.; Shi, J. Experimental and Simulation Study on a Catalyst Packed Tubular Dense Membrane Reactor for Partial Oxidation of Methane to Syngas. *Chem. Eng. Sci.* **2000**, *55*, 2617.

(37) Ritchie, J. T.; Richardson, J. T.; Luss, D. Ceramic Membrane Reactor for Synthesis Gas Production. *AIChE J.* **2001**, *47* (9), 2092.

(38) Tsai, C.; Dixon, A. G.; Moser, W. R.; Ma, Y. H. Dense Perovskite Membrane Reactors for Partial Oxidation of Methane to Syngas. *AIChE J.* **1997**, *43* (11A), 2741.

(39) Trimm, D. L. The Formation and Removal of Coke from Nickel Catalyst. *Catal. Rev.—Sci. Eng.* **1977**, *16* (2), 155.

(40) Bartholomew, C. H. Carbon Deposition in Steam Reforming and Methanation. *Catal. Rev.—Sci. Eng.* **1982**, *24* (1), 67.

(41) Uemiya, S. State-of-the-art of Supported Metal Membranes for Gas Separation. *Sep. Purif. Methods* **1999**, *28* (1), 51.

(42) Shu, J.; Grandjean, B. P. A.; Kaliaguine, S. Methane Steam Reforming in Asymmetric Pd− and Pd−Ag/porous SS Membrane Reactors. *Appl. Catal. A* **1994**, *119*, 305.

Received for review April 19, 2002
Revised manuscript received August 29, 2002
Accepted September 6, 2002

IE0202928